23

Magnesium Alloys Based Composites

Zuzanka Trojanová[1], Zoltán Száraz[2],
Peter Palček[3] and Mária Chalupová[3]
[1]*Charles University, Prague*
[2]*Joint Research Centre, European Commission, Petten*
[3]*University of Žilina*
[1]*Czech Republic*
[2]*The Netherlands*
[3]*Slovak Republic*

1. Introduction

Metal matrix composites offer a wide range of opportunities for many structure applications because of their improved mechanical properties in comparison with their monolithic metal counterparts. Light alloys reinforced with short fibres or particles allow adapting more exactly the work piece material properties to requirements. There is an increasing trend in the automotive industry to use these materials for various components. Advanced properties of metal matrix composites are:

- increased apparent limit of elasticity, stiffness, tensile and fatigue strength,
- improved creep resistance and high temperature properties,
- improved material damping,
- increased wear resistance,
- decreased thermal expansion.

Metal matrix composites (MMCs) based on magnesium alloys are excellent candidates for engineering light structure materials, and have great potential in automotive, high performance defence and aerospace applications. In spite of relatively high number of papers dealing with microstructure and mechanical properties of MMCs based on Mg alloys, the deformation mechanisms and other physical properties of these materials are not known enough. It has already been shown that the reinforcing fibres and/or particles improve mechanical and creep properties of magnesium based MMCs compared to their monolithic counterparts. But also the disadvantage of higher production costs due to more complicated manufacturing processes has to be taken into account (Dieringa et al., 2005). Only the use of cheap materials - both the alloy and the reinforcement – in relation to cost effective production processes for manufacturing of magnesium based MMCs can introduce this class of low density materials into the market. The objective of this chapter – following from this fact – is to reveal influence of various reinforcement types on the mechanical and physical behaviour of composites in which various magnesium alloys were reinforced with short alumina (Saffil®) fibres and/or SiC and Si particles. Different routs for magnesium based MMCs preparation were used:

i. Squeeze casting – the melt is infiltrated into the prefabricated perform (fibres and/or particles with some binder). The preform is preheated to 800–1000 °C in order to avoid

solidification during the infiltration process. The melt (in the case of Mg alloys) is superheated to a temperature between 700 and 720 °C and poured over the preform. The vertical stamp squeezes the melt under a pressure of about 60 MPa into the preform and the solidification takes approximately one minute. After the infiltration, the solidification process occurs under the pressure which leads to the fine microstructure without porosity and residual gases.

ii. Gas pressure infiltration – similarly as in the case of the squeeze casting the melt is infiltrated into the perform and the pressure is applied using the inert gas (argon).

iii. Powder metallurgy - Gas atomised alloy powder and SiC particles were mixed in an asymmetrically moved mixer with subsequent milling in a ball mill. In order to obtain an optimum dispersion of reinforcement in the matrix it is necessary to assure a certain particle/matrix powder size ratio. The maximum powder size was fixed at 63 μm. The powder was encapsulated in magnesium containers and extruded at 400 °C using a 400 t horizontal extrusion press.

A commercially available AZ91 magnesium alloy with the nominal composition Mg – 9%Al; 1%Zn; 0.3%Mn, in weight percent was reinforced by various reinforcement: 20 vol % of short Al_2O_3 (Saffil®) fibres (AZ91f), 15 vol.% of short Saffil fibres and 5 vol.% of SiC particles (AZ91h), further samples contained 10% SiC particles and an addition of 3wt.% Si (AZ91p). Composites were prepared by the squeeze casting method. The preforms consisted Al_2O_3 short fibres showing a planar isotropic fibre distribution and a binder system (containing Al_2O_3 and starch). Thermal treatment T6 was used (homogenisation for 18 h at 413 °C, then precipitation for 8 h at 168 °C). Samples of AZ91f were cut from the bulk with two orientations with respect to the fibre plane: the sample with the fibre plane parallel to the stress axis (AZ91f||) and perpendicular to the stress axis (AZ91f⊥). The mean Saffil fibre length and fibre diameter measured after squeeze casting were 78 and about 3 μm, respectively. The sharply shaped SiC particles in the AZ91h composite had a size of about 10 μm. The size of the SiC particles in the AZ91p composite was about 20 μm. Figure 1 shows the microstructure of undeformed AZ91f composite. It can be seen that many fibres are broken as a consequence of the squeeze casting procedure. The cut has been performed perpendicular to the fibres plane; 2D random distribution of fibres is well visible. Typical features of the microstructure are a solid solution of Al in Mg (δ-phase) and the γ-phase ($Mg_{17}Al_{12}$) intermetallic compound. Figure 2 shows the structure of AZ91h hybrid composite. The observed microstructure consists from δ-phase, electron compound $Al_{12}Mg_{17}$ (γ-phase) and discontinuous precipitate (lamellae of γ+δ phase). From the micrograph it can be seen that SiC particles are distributed non-uniformly. A representative view of the AZ91p composite with the addition of 3%Si and 10vol.% of SiCp is shown in Figure 3. The microstructure of AZ91 matrix (see Fig.3) consists of the δ-phase, the γ-phase and the discontinuous precipitate (lamellae of γ+δ phase). The addition of 3%Si gives rise to the Mg_2Si phase formed as eutectic Chinese script type particles, or primary Mg_2Si coarse dendrites. The Mg_2Si phase is present usually in the interior of δ-phase grains, and often islands of the entrapped δ-phase are present in some Mg_2Si coarse dendrites. The γ-phase is distributed mainly around grain boundaries and lamellae discontinuous precipitate was often adjacent to the γ-phase or grain boundaries. A typical feature of the microstructure of AZ91p composite is a small grain size of about 3 μm. Sharply shaped SiC particles with a size of about 9 μm are not uniformly distributed.

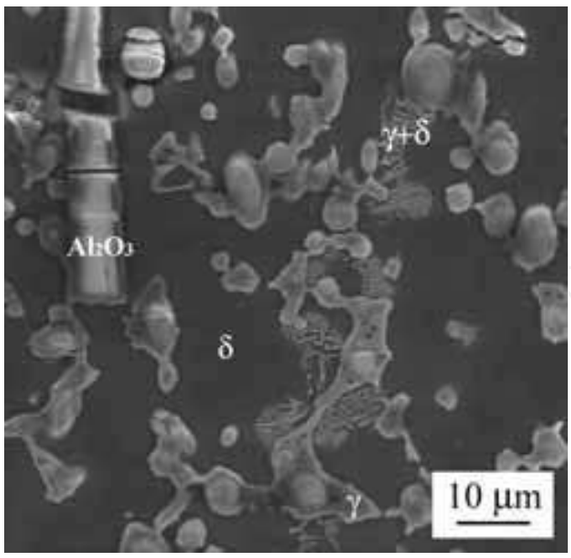

Fig. 1. Scanning electron micrograph of AZ91f MMC.

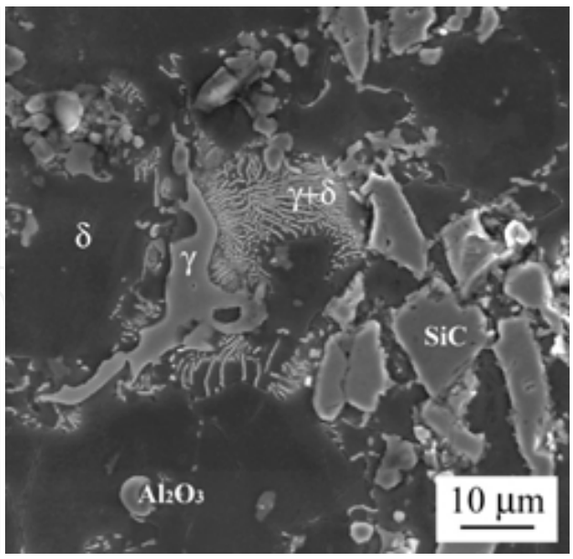

Fig. 2. Scanning electron micrograph of AZ91h MMC.

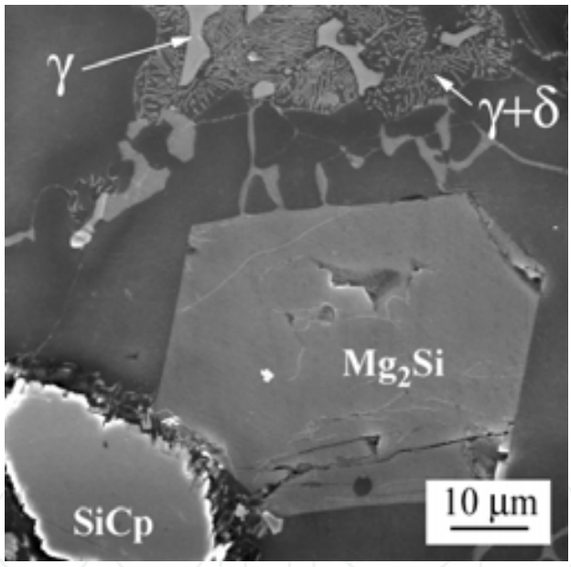

Fig. 3. Scanning electron micrograph of AZ91p MMC.

The microstructure of AZ91 matrix (see Fig.3) consists of the δ-phase, the γ-phase and the discontinuous precipitate (lamellae of γ+δ phase). The addition of 3%Si gives rise to the Mg_2Si phase formed as eutectic Chinese script type particles, or primary Mg_2Si coarse dendrites. The Mg_2Si phase is present usually in the interior of δ-phase grains, and often islands of the entrapped δ phase are present in some Mg_2Si coarse dendrites. The γ phase is distributed mainly around grain boundaries and lamellae discontinuous precipitate was often adjacent to the γ-phase or grain boundaries. A typical feature of the microstructure of AZ91pm composite is a small grain size of about 3 μm. Sharply shaped SiC particles with a size of about 9 μm are not uniformly distributed.

Commercial AS21 (2.2Al-1Si-0.1Mn-balance Mg-in wt%) alloy was used as the matrix material for composites with 30 vol.% short fibres of δ-Al_2O_3 (Saffil®) (hereafter AS21(f)) and hybrid composite with 5 vol.% of Saffil short fibres and 15 vol.% of SiC particles (AS21h). Composites were prepared using squeeze casting. The light micrograph of the AS21f composite is introduced in Fig. 4a.b. Planar random orientation is well visible in micrographs taken from two perpendicular sample surfaces. Characteristic feature of the composite microstructure is MgSi phase having a form of the dendritic crystals or characteristic Chinese-script. Microstructure of the AS21h hybrid composite consists of Saffil fibres. SiC particles and Mg_2Si particles.

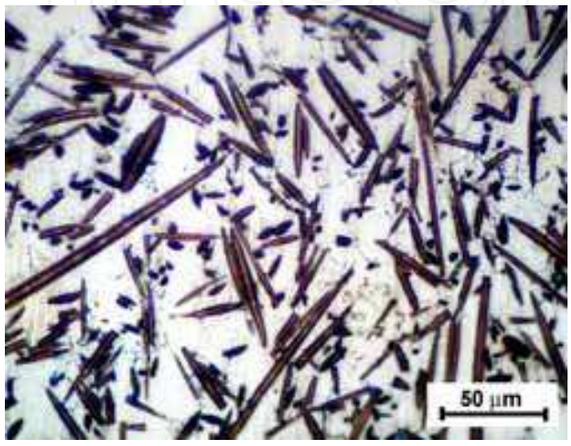

Fig. 4a. Light micrograph of AS21f MMC.

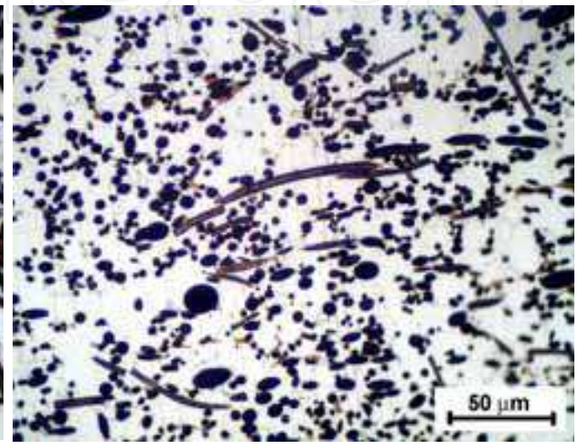

Fig. 4b. Micrograph from the perpendicular surface plane of the same sample as in Fig. 4a.

AX41 alloy (Mg – 4 wt.% Al – 1 wt.% Ca) reinforced with 13% Saffil fibres (AX41f) was prepared by squeeze casting technology. A typical feature of the AX41 alloy consists from solid solution of Al in Mg, α-Mg grains decorated by particles. SEM showed $Mg_{17}Al_{12}$ intermetallic phase surrounded with smaller particles of Al_2Ca. The microstructure of the composite is more complicated as it can be seen in Fig. 5.

Light Mg-Li alloys are attractive candidates for reinforcement with ceramic fibres or particles. Pure Mg has hcp structure. The density of Mg-Li alloy decreases with an increase of lithium content. The addition of Li increases ductility. The Mg-Li phase diagram shows that Li is soluble in hcp α phase up to 4 wt.%, while Mg alloyed with greater than 12 wt% Li has a bcc structure. Mechanical properties of the hcp α phase are worse in comparison with the *bcc* alloys, which are very good machinable and weldable. Disadvantages of Mg-Li alloys with *bcc* structure are a high chemical activity and poor corrosion resistivity. Some compromise would be an alloy with 8 wt% of Li (a mixture of phases α+β), which might exhibit both improved mechanical properties as well as a good corrosion resistance. Further improvement of mechanical properties is possible if the alloy is reinforced with the ceramic fibres or particles. Mg-xLif composites reinforced with Saffil fibres were produced by the gas pressure infiltration of evacuated fibrous preform with metallic melt in the autoclave. The mean fibre length and fibre diameter after infiltration was ~100 μm and ~3 μm, respectively. Microstructure of the as prepared Mg-4Lif sample is shown in Fig. 6. The structure of as-cast Mg-8Lif alloys under consideration consists essentially of *hcp*

magnesium-based α-phase (lighter) and *bcc* lithium-based β-one (darker). Accordingly, interpenetrated (α+β) matrix structure with dominating α-phase is characteristic of short δ-Al_2O_3 fibre reinforced Mg-8Lif composites wherein the fibres are planar randomly distributed within α and β matrix regions (Fig.7).

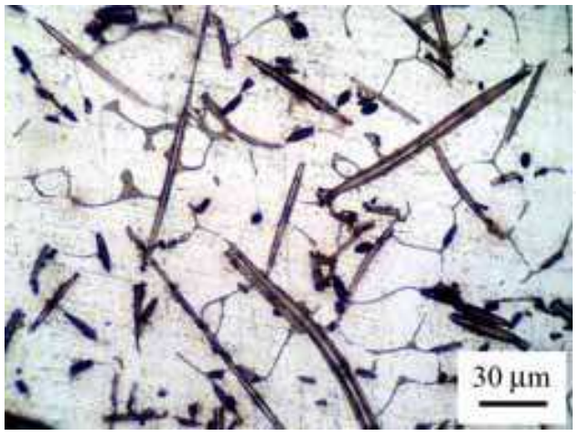

Fig. 5. Light micrograph of AX41f MMC.

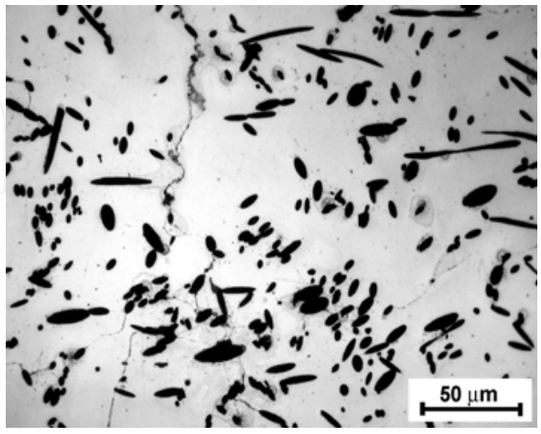

Fig. 6. Light micrograph of Mg-4Lif MMC.

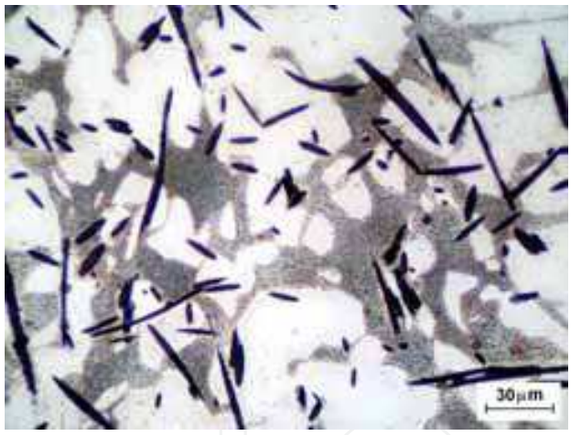

Fig. 7. Light micrograph of Mg-8Lif MMC.

An example of the microstructure of the composite reinforced with particles, prepared by a powder metalurgy method is introduced in Fig. 8. The WE54 alloy (Mg–5%Y–4%RE) was reinforced by 13vol.% SiC particles. The micrograph in Fig. 8 was taken perpendicularly to the extrusion direction. SiC particles are non-uniformly distributed in the matrix; they form in many cases small clusters. The typical feature of the powder metallurgic composites is the small grain size, smaller than the size of the reinforcing particles. The size of sharp bounded more or less uniaxial particles is in this case approximately 9 μm and the grain size in the matrix about 3-4 μm. Light micrographs and scanning electron micrographs showed no pores in the composite and the binding between SiC particles and the matrix was perfect. No defects were found in the vicinity of SiC particles and no chemical reaction at the interface matrix/SiC particles was observed. The same method was used for preparing of the composite based in Mg-8Li alloy with 7 vol. % of SiC. From the micrograph taken from

the cross section, shown in Fig. 9, it is obvious that the matrix microstructure has two phases. The light *a* phase (hcp solid solution of Li in Mg) and the dark β phase (bcc solution with the higher content of Li). The X–ray analysis revealed the relation between both phases as α : β = 55 : 45. As the grain size the mean value of 5±2 μm was taken from both phases. The size of sharp bounded more or less equiaxial SiC particles was approximately 9 μm. The distribution of particles is not uniform; small clusters of SiC particles are present similarly as in the case of other composites prepared in this way.

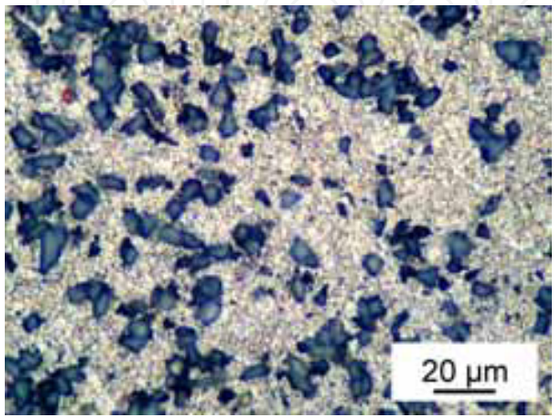

Fig. 8. Light micrograph of WE54/ SiC.

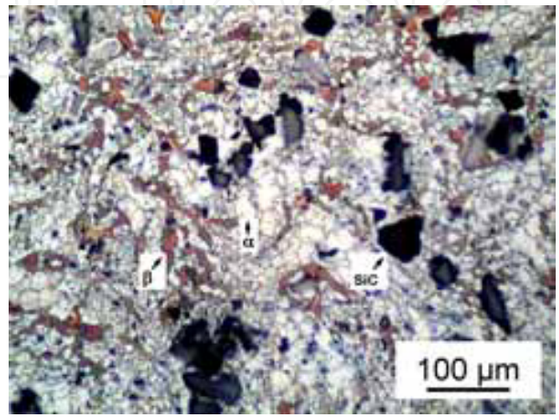

Fig. 9. Light micrograph of Mg-8Li/ SiC.

2. Mechanical properties

Physical properties of composites are affected by properties of individual constituents, by properties of the matrix and the reinforcing phase. The volume fraction, geometry and distribution of reinforcement influence dislocation behaviour and the mechanical properties of composites. Reinforcement may also influence other material properties as the wear resistance or damping capacity. Mechanical properties of composites are determinate not only by properties of matrix and the reinforcing phase, but also with their interaction. It is well established that the microstructure and the mechanical properties of MMCs are strongly affected by the nature of the interfaces between the matrix and the reinforcement. Generally, week bonding between them worsen their properties. Another important factor is the preparation method (powder metallurgy, squeeze casting, etc.).

Composites are inhomogeneous in both elastic as well as plastic properties. While the reinforcing phase remains usually only elastically deformed due to mechanical loading of composites, the plastic deformation occurs in the matrix. Geometry and distribution of the reinforcement have a great influence on the localization of the deformation during straining. Ductility of the composites decreases rapidly with increasing volume fraction of the reinforcement and significantly reduced compared to unreinforced alloys (Lloyd, 1994). The addition of the reinforcing phase increases the yield stress and strength of composite materials. Strengthening in metals and alloys reinforced by fibres or particles were analysed in many papers with the aim to find the correlation between mechanical properties and microstructural characteristics of composites. In spite of many attempts there is no generally accepted model for MMC strengthening. It is probably due to very complex character of the

problem. Many factors and mechanisms play role and synergetic operation of these mechanisms has been not sufficiently studied.

It is not straightforward to propose theoretical model including all deformation mechanisms predicting mechanical properties of given composite. Individual models take into account only some mechanisms and influence of other mechanisms is neglected. However, we can estimate contribution of various factors and to establish the most important mechanism (-s).

Flow stress, necessary for deformation of the composite is affected with different processes and is a superposition off different contributions:

- load transfer from matrix to fibres;
- enhanced dislocation density due to different elasto-plastic and thermal properties; of the matrix and the reinforcing phase;
- Orowan strengthening;
- residual thermal stresses in the matrix;
- grain boundary hardening. Discontinuously reinforced composites usually have finer grains than the unreinforced alloy.

2.1 Hardening mechanisms

Load transfer

For interpretation of the strengthening effect of long fibres embedded homogeneously in a continuous weak matrix and aligned parallel to the stress axis the shear-lag theory was proposed by Cox (Clyne & Withers, 1993). This theory assumes that if no slip occurs on the matrix-fibre interfaces, transfer of the applied load from the matrix to the fibres occurs by the shear stresses acting on the fibre/matrix interface. The presence of the fibre redistributes the stresses and strains within the composite material. The harder reinforcement carries greater part of the stress, while the soft matrix tends to take the greater part of the deformation. This model gives prediction of the axial tensile stress in fibres and the shear stresses at the fibre-matrix interface during axial straining. The shear lag model is based on the simplifying assumption of uniform matrix deformation and, therefore, it yields a very simplified expression for stiffness and strength contribution. Except for the stress transfer from the matrix to the fibres, the shear lag model does not account for the contributions from effects, which are associated with the anisotropic matrix behaviour, resulting in enhanced dislocation density and residual thermal stresses. In the original model of Cox, the load transferred from the matrix to the end faces of the fibre is ignored. However, for short fibre lengths the tensile transfer of load cannot be neglected because the aspect ratio significantly affects the predicted composite strength. In order to overcome this shortcoming of the original model, modifications of the original model have been made by several authors. The contribution of the load transfer when the fibres are aligned parallel to the applied stress is then done by the following equation (Aikin & Christodoulou, 1991):

$$\Delta\sigma_{LT} = \sigma_y\left(\frac{(L+t)A}{4L}\right)f \tag{1}$$

where σ_y is the stress in the matrix, L the fibre length in the stress direction, t the fibre diameter, A the fibres aspect ratio A = L/t, and *f* is the volume fraction of reinforcing fibres in the matrix. From the Eq. (1), it follows that possible influence of particles (with the same

volume fraction) may be weaker due to low value of the aspect ratio A. For equiaxial particles, an increase in the deformation stress due to load transfer may be given by:

$$\Delta\sigma_{LT} = 0.5\sigma_y f \tag{2}$$

Enhanced dislocation density due to thermal mismatch

In MMCs higher dislocation density was observed than in the unreinforced alloy (Arsenault & Fisher, 1983). The thermoelastic properties are different for reinforcement and matrix and therefore temperature changes will cause misfit between them. Typically, the coefficient of thermal expansion (CTE) of the metallic matrix is higher than CTE of the ceramic reinforcement. When the metal matrix composite is cooled from a higher temperature to room temperature, misfit strains occur because of differential thermal contraction at the matrix-reinforcement interface. These strains induce thermal stresses that may be higher than the yield stress of the matrix. Thermal stresses arising from the cooling of the composites from the processing temperature can be partially released by plastic relaxation, i.e. by dislocation generation in the vicinity of the interface. This leads to the formation of a high dislocation density in the matrix, hence to higher yield strength. The density of newly formed dislocations, near reinforcement can be calculated as (Arsenault & Shi, 1986):

$$\Delta\rho_T = \frac{Bf\Delta\alpha\Delta T}{b(1-f)}\frac{1}{t'} \tag{3}$$

where B is a geometrical constant (B = 10 for fibres and B = 12 for particles), b is the magnitude of the Burgers vector of the newly created dislocations, t′ is a minimum size of the reinforcing phase particles or fibres, Δα is the difference between the two thermal expansion coefficients and ΔT the temperature variation.

When the thermal stresses achieve the yield stress, plastic zones can be formed in the matrix near the interfaces, especially, in the vicinity of fibre ends.

With addition of the reinforcing phase, the geometrically necessary dislocations are generated to accommodate the mismatch of plastic deformation in the matrix. The density of the geometrically necessary dislocations may be expressed as (Ashby, 1993):

$$\Delta\rho_G = \frac{f8\varepsilon_p}{bt'} \tag{4}$$

where ε_p is the plastic strain. The influence of the geometrically necessary dislocations increases with increasing strain.

The strengthening in the matrix is attributed to the deformation resistance induced by the reinforcing phase. According to Taylor relation, the contribution to the total stress due to the presence of dislocations in the matrix may be written:

$$\Delta\sigma_D = \alpha_1\Psi Gb\left(\Delta\rho_T + \Delta\rho_G\right)^{1/2} \tag{5}$$

where α_1 is a constant, ψ is the Taylor factor and G is the shear modulus. This higher dislocation density as well as the reinforcement/matrix interfaces can provide high diffusivity paths in a composite. The higher dislocation density would also affect the precipitation kinetics in a precipitation hardenable matrix.

Orowan strengthening

The yield stress is characterized by the state when the matrix plastic flow is developed. Reinforcements (fibres, particles) in the matrix are obstacles for dislocation motion. Therefore, the stress necessary for motion of dislocations in the composite is higher than in the matrix without reinforcement. We consider a similar mechanism as in the case of strengthening by incoherent particles, i.e. Orowan strengthening. The gliding dislocation bows out between inclusions, and then bypasses them leaving a loop around them. The reinforcements also accumulating dislocations during deformation, thus internal stress is generating. Aside from reinforcements, dislocations may overcome these stress fields from dislocation pile-ups. Increase in the yield stress caused by this mechanism, in the first approximation, can be expressed as (Lilholt, 1991):

$$\Delta\sigma_{OR} = \frac{Gb}{\Lambda} + \frac{5}{2\pi} Gf\varepsilon_P \,, \tag{6}$$

where Λ is the inclusion spacing and ε_p is the plastic deformation.

Grain size refinement

Grain boundaries play important role in strengthening of polycrystalline metals. At low temperatures grain boundaries impede dislocation motion, thus strengthening the material. Impeding dislocation movement increases the stress required to continue the deformation process from grain to grain and hence increase the yield strength of the material. When the deformation rate and grain size are constant during the deformation than the effect of grain boundaries on strengthening is constant. The relation between yield stress and grain size is described by the Hall-Petch equation. Decreasing grain size increases the yield stress. Discontinuously reinforced composites usually have very fine grains, smaller than their unreinforced matrices (Trojanová et al., 2007). The contribution to the yield stress can then be estimated using the relation:

$$\Delta\sigma_{GS} = K_y\left(d_2^{-1/2} - d_1^{-1/2}\right) \tag{7}$$

Residual thermal stresses

At higher temperatures, internal stresses can achieve the yield stress and the composite is plastically deformed only owing to the temperature cycling. Thermal stresses directly in the matrix/fibre interface may be calculated in the simple approximation as (Carreño-Morelli et al., 2000):

$$\sigma_{TS} = \frac{E_f E_m}{(E_f f + E_m(1-f))} f\Delta\alpha\Delta T \tag{8}$$

where E_f and E_m are Young's moduli of the reinforcing phase (fibres or particles) and the matrix, respectively. In a certain distance r from the fibre the thermal stress is lower because it decreases with the distance as $1/r^3$. Thermal stresses arising at higher temperatures can be partially accommodated inducing new dislocations. Residual thermal stresses exist also at ambient temperature and relax very slowly (Miller & Humphreys, 1991). These stresses in the matrix are tensile ones; they may increase the stress necessary for compressive deformation of the composite. Volume-averaged stresses can be estimated by averaging the

local stresses predicted in a representative volume element. Volume-averaged residual stresses in the matrix reach their maximum value (Delannay, 2000):

$$\langle \sigma_m \rangle_{max} = \frac{2}{3}\sigma_y \ln\left(\frac{1}{f}\right)\frac{f}{1-f} \tag{9}$$

Combination of strengthening terms

Several schemes have been proposed for addition of the various strengthening terms. The most commonly accepted are those reviewed by Lilholt (Clyne & Withers, 1993), who differentiates between the range of magnitude of the strengthening mechanisms and their relative strength. In principle, computer models are required to sample statistically the different contributions. Clearly, stress contributions, which act more or less uniformly throughout the matrix must be superimposed linearly, whereas mechanisms of similar strengthening ability, which act unevenly throughout the matrix, are most suitably combined as the root of the sum of the squares.

2.2 Experimental results

Composites based on AS21, AX41, AX61, AZ91, Mg-4Li, Mg-8Li, and WE54 perspective magnesium alloys were investigated. AS21f, AX41f, AX61f and AZ91f alloys were reinforced with short δ-Al_2O_3 (Saffil) fibres. In case of AX41 alloy also Sigrafil C40 short fibres were used as reinforcement. AZ91p, Mg-8Lip and WE54p alloys were reinforced with equiaxed SiC particles. The hybrid composites AS21h and AZ91h were reinforced with short fibres and SiC particles. The type and the volume fraction of the reinforcement are introduced in the Table 1. Specimens for the compression test had cylindrical or rectangular shape. Specimens of composites, reinforced with Saffile fibres, were cut from the bulk with two orientations with respect to the fibre plane: the sample with the fibre plane parallel (||) to the stress axis and perpendicular to the stress axis (⊥).

Alloy	Volume fraction of reinforcement. %			Notation
	Saffil	SiC	Sigrafil	
AS21	30	–	–	AS21f
AS21	5	15	–	AS21h
AX41	13	–	–	AX41f
AX41	–	–	25	AX41S
AX61	26	–	–	AX61f
Mg-4Li	10	-	-	Mg-4Lif
AZ91	20	–	–	AZ91f
AZ91	15	5	–	AZ91h
AZ91	–	10	–	AZ91p
Mg-8Li	–	7	–	Mg-8Lip
WE54	–	13	–	WE54p

Table 1. Volume fraction of reinforcements in composites investigated.

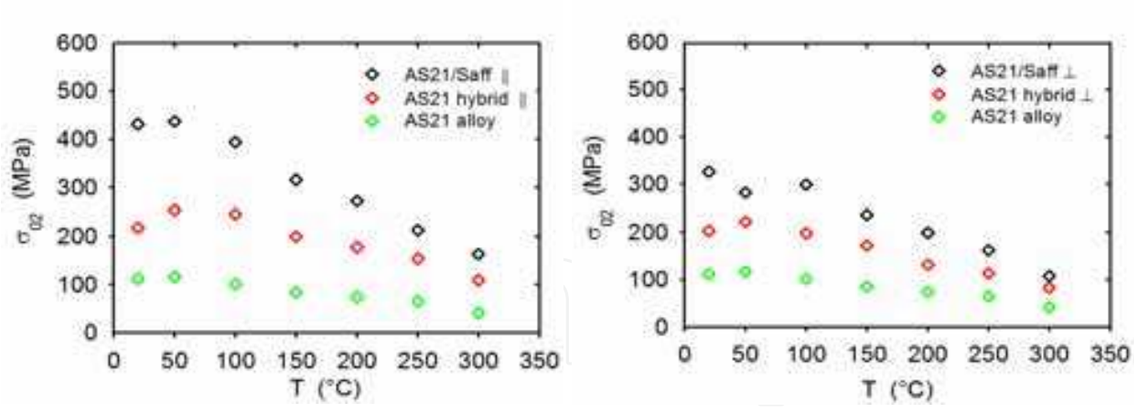

(a) (b)

Fig. 10. Comparison of the yield stress σ_{02} for AS21f, AS21h MMCs and the matrix alloy AS21 in parallel orientation (a) and perpendicular orientation (b)

Ceramics fibres and particles significantly influence the mechanical properties of composites. The flow stress and the maximum stress are higher for composites than those for unreinforced alloy. The influence of the reinforcing phase on the yield stress is well apparent from figure 10 and for the maximum stress in figure 11 where the characteristic stresses for AS21h, AS21f and unreinforced AS21 alloy are introduced depending on temperature. Anisotropy in the mechanical properties of fibre reinforced composites was found. Parallel orientation of the fibres plane in composites markedly increases characteristic stresses. This fibres impact decreases with increasing temperature. It can be seen the major effect of fibres in comparison with particles. For composites reinforced with equiaxial particles the load transfer plays marginal role. Anisotropy of the hybrid composite is lower but not negligible.

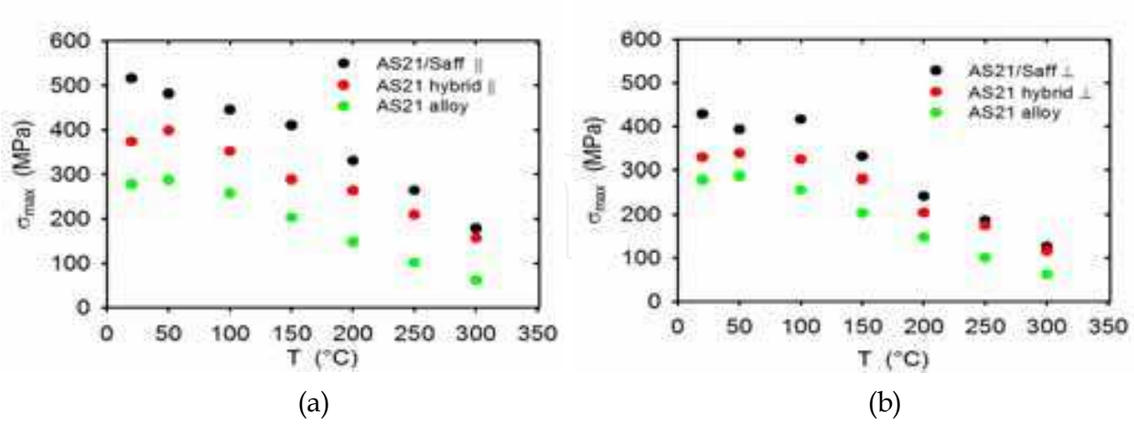

(a) (b)

Fig. 11. Comparison of the maximum stress σ_m for AS21f, AS21h MMCs and the matrix alloy AS21 in parallel orientation (a) and perpendicular orientation (b)

The main disadvantage in the mechanical properties of MMCs is their limited ductility. The elongation decreases rapidly with the addition of reinforcing phase. The quality of the interface between the particles and the matrix, the particle size, distribution and volume

fraction influence the composite ductility. Higher ductility for a given volume fraction of the particles is possible to achieve with (Lloyd, 1994):

- uniform particle distribution;
- using fine (<10 μm) particles;
- high interfacial strength;
- controlling the particle shape;
- using of ductile matrix.

Various strengthening mechanisms which can operate in MMCs were described in section 2.1. Individual contributions to the strengthening for composites AS21f, AX41f, Mg-4Lif, AX41S, AX61f, AZ91f, AZ91h, AZ91p, Mg-8Lip a WE54p, calculated using constants introduced in Table 2 and 3, are summarized in Table 4. Contributions were evaluated at room temperature in the vicinity of the yield stress (plastic strain ε_p = 0.002). The combination of individual strengthening terms gives the increase in the yield stress with addition of the reinforcing phase into the matrix. In case of fibre reinforced end hybrid composites the contributions were calculated for parallel fibre orientation. Difference between two orientations is in the load transfer. For fibres oriented perpendicular to the compression axis the transfer of the load from the matrix to the fibres is not effective.

From Table 4 it follows that the load transfer ($\Delta\sigma_{LT}$), in which the part of the external load within the matrix is transferred to reinforcement, is important strengthening mechanism in the composites reinforced by short fibres (see also Trojanová et al., 2007, 2008). On the other hand, this mechanism is in the particle reinforced composites marginal. From the Eq. (1), it follows that possible influence of particles (with the same volume fraction) may be weaker due to low value of the aspect ratio A. Enhanced dislocation density may also significantly increase the yield stress in the composites reinforced with short fibres.

AS21	AX41	AX61	AZ91	Mg-4Li	Mg-8Li	WE54	Saffil	SiC
26	25	25	26	26	30	26	26	6.6

Table 2. Linear thermal expansion coefficients $\alpha \times 10^6$ in K^{-1} used for calculations of values in Table 4.

K_y (*hcp*) ($MPam^{-3/2}$)	K_y (bcc) ($MPam^{-3/2}$)	b (m)	G (GPa)	Taylor factor	α_1
0.28	0.2	3.2×10^{-10}	17	6	0.35

Table 3. Constants used for calculations of values in Table 4.

The higher dislocation density is a consequence of the difference between the thermal expansion coefficients of both phases. Enhanced dislocation density was a common feature for all non-deformed composites. Fig. 12 is showing high dislocation density in as-received composites AS21f and WE54p. As it follows form the Table 4, the Orowan mechanism play only marginal role for the composites strengthening. Orowan strengthening for reinforcing particles is not significant for the selected composites, because the particles are coarse and the inter-particle spacing exhibits several μm (see also Száraz et al., 2007).

The main hardening mechanism seems to be the small grain size of the materials prepared by the powder metallurgical route. Smaller matrix grain size also reduces twinning which is important deformation mode in the coarse grained hcp materials. The grain size refinement does not play important role in the strengthening of fibre reinforced composites where the load transfer mechanism plays the significant role.
Thermal stresses arising due to a high difference between the thermal expansion coefficients can be partially accommodated by dislocation generation in the matrix. Residual stresses exist also at ambient temperature and they relax very slowly. Residual thermal stresses have at ambient temperature tensile character and they may increase the stress necessary for compressive deformation of the composite. Maximum values of the volume-averaged residual stresses in the matrix are introduced in Table 4. The increase in the composite yield strength was estimated as a linear combination of individual strengthening terms. Comparison with the experimental result shows that the theoretically predicted values of σ_{02} introduced in table 4 are in very good agreement wit the experimental measured values.

Composite	$\sigma_{02alloy}$ (MPa)	$\Delta\sigma_{LT}$ (MPa)	$\Delta\sigma_{D}$ (MPa)	$\Delta\sigma_{OR}$ (MPa)	$\Delta\sigma_{GS}$ (MPa)	$\langle\sigma_m\rangle_{max}$ (MPa)	σ_{total} (MPa)	$\sigma_{02exp.}$ (MPa)
AS21f	112	136	84	8	12	39	391	432
AX41f	68	36	51	2	15	14	186	168
AX41/S	83.5	51.5	57.3	2	17	25.7	237	248
AX61f	84	89	79	7	23	27	309	322
Mg-4Lif	69	36	48	3	17	12	185	251
AZ91f	116	94	55	5	25	31	326	324
AZ91h	116	32	38.4	5	15	31	237.4	267
AZ91p	116	9	24	0	96	26	271	222.5
Mg-8Lip	85	3	17	0	101	13	219	198
WE54p	140	11	28	4	52	28	263	246

Table 4. Contributions of various strengthening mechanisms to the yield stress of the selected composites at room temperature.

It is well established that the microstructures and the mechanical properties of MMCs are strongly affected by the nature of the interfaces between the matrix and the reinforcement. (Models are constructed for perfect bonding between the reinforcement and the matrix.) Moreover, individual models take into account only some strengthening mechanisms and influence of other mechanisms are neglected. Nevertheless, we can estimate contribution of various factors and establish the most important mechanism.

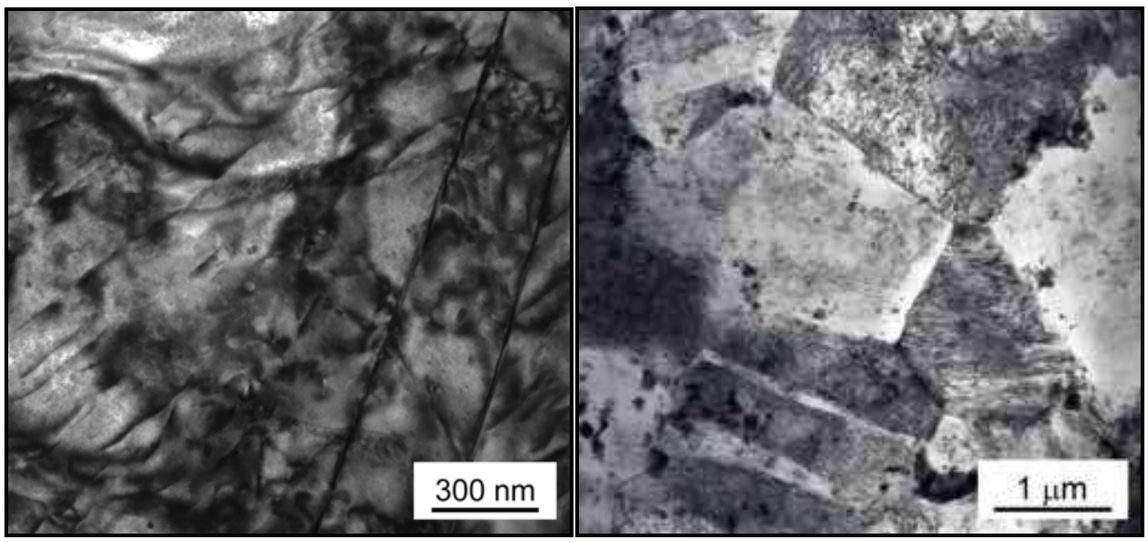

(a) (b)

Fig. 12. TEM micrographs showing high dislocation density in non deformed AS21f (a) and WE54p (b) samples.

Concluding remarks

Ceramics fibres and particles significantly influence the mechanical properties of composites. The flow stress and the maximum stress are higher for composites than those for unreinforced alloy.

Investigations revealed that the high dislocation density is a common feature for both non-deformed and deformed composites. Dislocations in the matrix of the non-deformed composites were induced during the fabrication process due to the large difference in the CTE of the matrix and ceramic reinforcement.

The main hardening mechanism in the composites strengthened with short fibres is the load transfer in which the part of the external load within the matrix is transferred to reinforcement. An increase in the dislocation density plays also important role.

High strength of the composites prepared by powder metallurgy may be attributed to the small grain size. Smaller matrix grain size also reduces twinning which is important deformation mode in the Mg alloys.

Thermal stresses arising due to a big difference between the thermal expansion coefficients may be partially accommodated by dislocation generation in the matrix. Tensile residual stresses exist also at ambient temperature. They have tensile character and in compression test increase the stress necessary for the plastic deformation. Other possible mechanisms play in strengthening only a marginal role.

3.2 High temperature properties

From Figs. 10 and 11 it can be seen that the strength of composites decreases with increasing temperature. The difference between the yield stress and the maximum stress decreases with increasing temperature. The stress-strain curves are very flat and the work-hardening rate $\vartheta = (d\sigma/d\varepsilon)$ exhibits small values. Physical processes responsible for plastic flow are similar to those occurring in creep.

Strain hardening in the matrix

The deformation behaviour of the composite can be explained under assumption that the macroscopic work-hardening rate is a result of two microscopic effects: storage and annihilation of dislocations. We should consider processes of storage of dislocations at both dislocation forest and non-dislocation obstacles (e.g. incoherent second phase particles, dispersoids, fibres). Assuming that the particle size and the spatial distribution of particles remain unchanged during deformation process we may consider two hardening and two softening processes. Lukáč and Balík formulated a constitutive model (Lukáč & Balík, 1994) giving the stress dependence of work hardening rate in the form

$$\vartheta = d\sigma/d\varepsilon = A/(\sigma-\sigma_y) + B - C(\sigma-\sigma_y) - D(\sigma-\sigma_y)^3 \quad (10)$$

where σ_y is the yield stress, A and B are parameters determined by impenetrable obstacles and forest dislocations, respectively, C and D express the dislocation annihilation due to cross slip and dislocation climb. While parameters A and B are virtually independent of temperature, C and D parameters are strongly temperature and strain rate dependent; increasing with increasing temperature and/or decreasing strain rate. The observed stress-strain curves can be correlated with Eq. (10). The analysis was performed for ZE41 alloy reinforced with 20 vol.% of Saffil fibres (Trojanová et al. 2004). Estimated parameters are shown in Table 5.

Temperature	A (MPa^2)	B (MPa)	C	D (MPa^{-2})	σ_y (MPa)	σ_{02} (MPa)	R^2
RT	114439	3078	33.12	4.43e-10	253	254	0.988
50 °C	164641	3984	42.07	6.28e-6	243	236	0.974
100 °C	143212	1106	22.67	1.85e-4	237	241	0.992
150 °C	334442	1164	93	9.18e-3	163	210	0.998

Table 5. Fit parameters in the equation (10).

From Table 5 it follows that the main dislocation obstacles are the impenetrable obstacles. The development of the dislocation density increases the storage probability of dislocations. With increasing temperature the storage probability should decrease. This could cause a decrease in the parameter B with temperature, which is indeed observed. The parameter C increases with temperature, which indicates that cross slip becomes a significant recovery process at higher temperatures. The parameter D increases with increasing temperature, which is expected in the case of climb. Similar results were found also in the case of other magnesium composites prepared by squeeze casting and gas pressure infiltration. Changes in the forest dislocation density (the density of dislocations in non-basal planes) can be expected with increasing temperature.

Cross slip recovery process

The variation of the flow stresses with increasing temperature may be accounted for by increasing activity of cross slip of dislocations. The values of the maximum stress could be, therefore, considered as characteristics of the cross slip activity. The maximum stress should then decrease with increasing temperature in similar way as the stress necessary for cross slip, i.e. the temperature dependence may be expressed by the following equation:

$$\ln \sigma_{max} = K_0 - K(\gamma, \dot{\varepsilon}) T \quad (11)$$

where K_0 is a constant and $K(\gamma, \dot{\varepsilon})$ is a function of the stacking fault energy γ and the strain rate $\dot{\varepsilon}$. Schematic representation of this mechanism is shown in Fig. 13a. Screw dislocations may cross slip from one basal plane through a non-basal plane (prismatic or pyramidal) and continue the movement in the parallel slip basal plane. The cross-slipped dislocations may eventually annihilate with the dislocations having the opposite sign.

(a) (b)

Fig. 13. Schematic diagram of cross slip of dislocation in the vicinity of a fibre (a) and dislocation reaction and climb of dislocations (b).

Local climb of dislocations

The moving dislocations cannot cut the fibres (or particles). The dislocations may pass the fibres leaving loops around the fibres. This athermal passing mechanism is similar to the Orowan mechanism. Dislocation pile-ups at the fibres can act as stress concentrators. Screw dislocation components locally cross slip forming superjogs having a height of about fibre diameter and at higher temperatures, edge components are able to climb. Both may then annihilate in neighbouring slip planes. Annihilation of dislocations may also be supported by diffusion of vacancies in the thin layer at the matrix-fibre interface. On the other hand, dislocations in the basal and pyramidal planes may interact forming the sessile dislocation according to reaction

$$\frac{1}{3}\langle 2\bar{1}\bar{1}3\rangle_{(2\bar{1}\bar{1}2)} + \frac{1}{3}\langle \bar{2}110\rangle_{(0001)} \rightarrow \langle 0001\rangle . \quad (12)$$

The resulting dislocation is not able to glide in the basal as well as pyramidal plane. Such dislocations may climb along the fibres as it is illustrated in Figure 13b. Local climb of dislocations may reduce the work hardening in the matrix and is very probably an important recovery process. With increasing temperature, the plastic strain rate is also increasing (diffusion increases with temperature exponentially). Accordingly, this mechanism influences the deformation behaviour of the composite.

3. Stres relaxation tests

Internal stress in the matrix

In alloys, the applied stress σ necessary for deformation of any polycrystalline material can be divided into two components: the internal (athermal) stress σ_i and the effective stress σ* i.e. one can write

$$\sigma = \sigma_i + \sigma^*. \quad (13)$$

In a composite the athermal component includes the stress which is necessary for deformation due to the load transfer σ_{LT} and σ_i^D the stress necessary for generation of dislocations, their movement and storage. The flow stress σ_{LT} necessary for composite deformation due to the load transfer which is done by the equation (1). The internal stress σ_i^D resulting from long-range internal stresses impeding the plastic flow is done as

$$\sigma_i^D = \alpha_1 G b \rho_t^{1/2}, \quad (14)$$

where α_1 is a constant describing interaction between dislocations and ρ_t is the total dislocation density. The effective shear stress, σ^*, acts on dislocations during their thermally activated motion when they overcome short range obstacles.

The internal stress increases due to dislocation storage in the matrix, $\sigma_i^D \propto \rho_t^{1/2}$, because the total dislocation density ρ_t increases due to two reasons: (a) generation of thermal dislocations and (b) the presence of dislocations geometrically necessary.

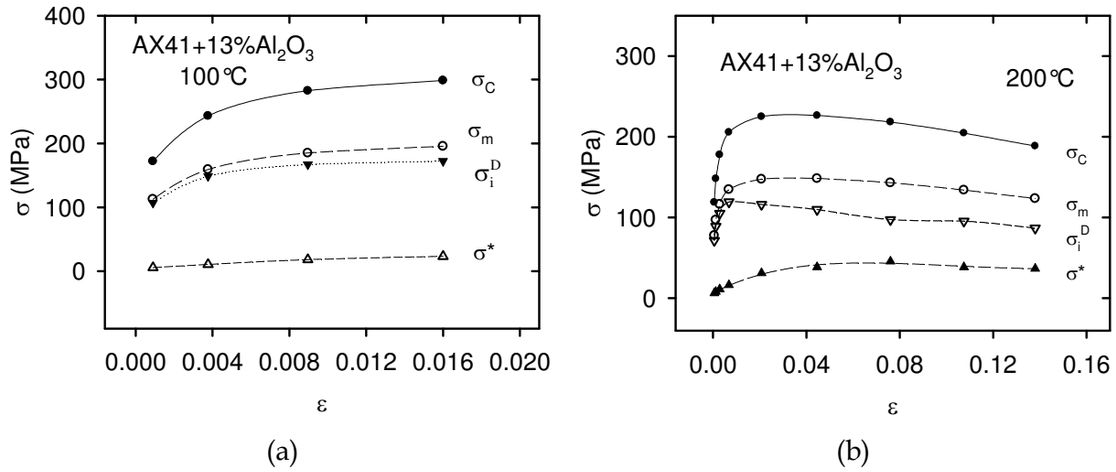

(a) (b)

Fig. 14. Part of the true stress-true strain curves obtained at 100 °C (a) and 200 °C (b). Points indicate the stresses at which the SR tests were performed.

The stress relaxation technique is very useful method to estimate the internal stress component and parameters of the thermally activated processes. In a stress relaxation (SR) test, the specimen is deformed to a certain stress σ_0 and then the machine is stopped and the stress is allowed to relax. The stress decreases with the time t. The specimen can be again reloaded to a higher stress (load) and the SR test may be repeated. The time derivative $\dot{\sigma} = d\sigma/dt$ is the stress relaxation rate and $\sigma = \sigma(t)$ is the flow stress at time t during the SR. The stress components (σ_i^D,σ^*) were estimated from the stress relaxation curves using the Li equation (Li, 1967). The SR curves were fitted to the power law function in the form: $\sigma - \sigma_i = [a(m-1)]^{\frac{1}{1-m}} (t + t_0)^{\frac{1}{1-m}}$, where a, t_0 and m are fitting parameters. A part of the stress strain-curve for AX41+13%specimens deformed at 100 °C is shown in Fig. 14a. Full circles depict points at the stress-strain curve where the stress relaxation tests were performed.

Blank circles indicate the matrix stress and full and blank triangles designate the internal stress, σ_i^D , and the effective stress, σ*, respectively. It is obvious that the internal stress, σ_i^D , is a substantial contribution to the matrix stress, σ_m. A similar analysis was performed at 200 °C and introduced in Fig. 14b. As it follows form Fig. 14b the internal stress increases with strain only in the very beginning of deformation; for strains higher than about 2%, it decreases with strain while the effective stress increases continuously up to a true strain of 8%. For higher strains, the effective stress remains constant, while the applied stress is decreasing. Comparison of the internal stress estimated for the AX41 alloy and that for the composite with the AX41 matrix reinforced with the 13% of Saffil fibres is introduced in Fig. 15. Subtracting the value of the load transfer, it can be seen that the internal stress level in the composite is higher than that in the unreinforced alloy. The difference exhibiting 64.5 MPa is due to a higher density of thermal dislocations (ρ_T=1.78x10^{13} m^{-2}) and dislocations geometrically necessary (ρ_G=1.4x10^{13}m^{-2}). Corresponding stress $\Delta\sigma_\rho = \alpha\psi Gb(\Delta\rho)^{1/2}$= 64.4 MPa.

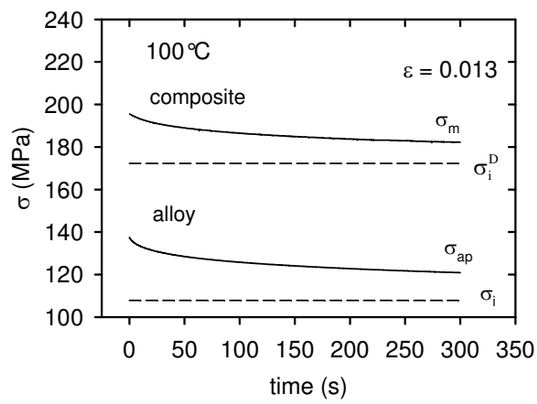

Fig. 15. A comparison of the dislocation internal stress estimated at 100 °C and at a strain of 0.013 for the composite and the monolithic alloy.

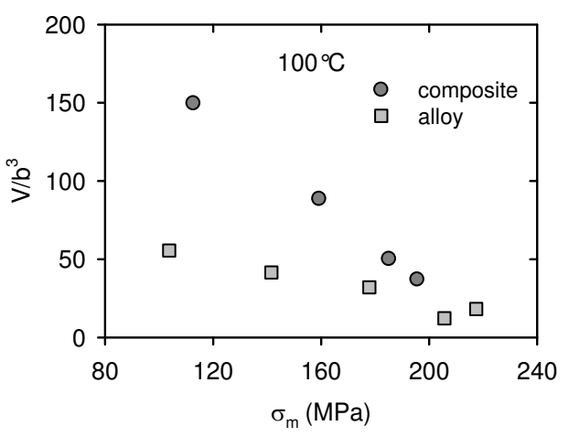

Fig. 16. Activation v volume in b^3 depending on the stress in the matrix estimated for the composite and the monolithic alloy.

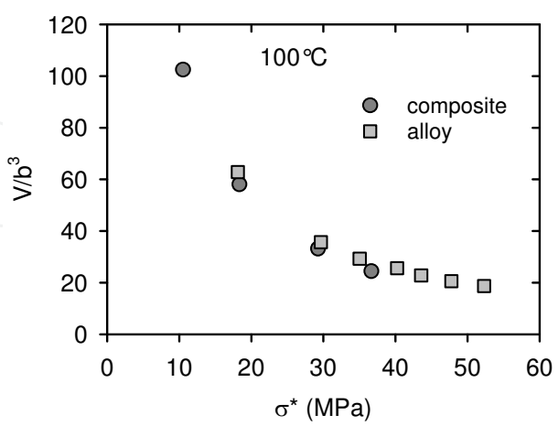

Fig. 17 The plot of the activation volume in b^3 against the effective stress estimated at 100 °C for the composite and the monolithic alloy.

Thermal activation

The stress decrease with the time during the SR test can be described by the well known Feltham equation (Feltham 1963):

$$\Delta\sigma(t) = \sigma_0 - \sigma(t) = \alpha\ln(\beta t+1), \tag{15}$$

where α and β are parameters. The dislocation activation volume V is given as $V=kT/\alpha$. The values of the apparent activation volume V_{app} were estimated according Eq.15 using stress decrease in the matrix $\sigma_m = \sigma_{app} - \Delta\sigma_{LT}$. As usual, the values of the activation volume were divided by b^3.

The values for samples deformed at 100 °C are plotted against the matrix stress σ_m in Fig. 16. For comparison, the values of the activation volume (divided by b^3) estimated for unreinforced alloy at temperature of 100 °C are also introduced. If the same values of the activation volume are plotted against the effective (thermal) stress σ^* all data lies on one line - "master curve" (Fig. 17). Kocks et al. (Kocks et al. 1975) suggested an empirical equation between the Gibbs enthalpy ΔG and the effective stress σ^* in the following form:

$$\Delta G = \Delta G_0\left[1-\left(\frac{\sigma^*}{\sigma_0^*}\right)^p\right]^q \tag{16}$$

where ΔG_0 and σ_0^* are Gibbs enthalpy and the effective stress without thermal activation, p and q are phenomenological parameters reflecting the shape of a resistance obstacle profile. The possible ranges of values p and q are limited by the conditions $0 < p \leq 1$ and $1 \leq q \leq 2$. Ono (Ono, 1968) and Kapoor (Kapoor et al. 2002), suggested that Eq (16) with p = 1/2, q = 3/2 describes a barrier shape profile that fits many predicted barrier shapes. Thermodynamics generally defines the activation volume as a derivative of the Gibbs potential with respect to the effective stress, i.e. $V = -(d\Delta G/d\sigma^*)_T$, then the equation (16) ca be rewritten as

$$V = \frac{\Delta G_0 pq}{\sigma_0^*}\left[1-\left(\frac{\sigma^*}{\sigma_0^*}\right)^p\right]^{q-1}\left(\frac{\sigma^*}{\sigma_0^*}\right)^{p-1}. \tag{17}$$

The values of the activation volume lie at the curve given by Eq (17), as it is obvious from Fig. 17. The activation enthalpy $\Delta H = \Delta G - T\Delta S$ (ΔS is the entropy) is done by $\Delta H = -TV(d\sigma/dT)$. The differential coefficient $d\sigma/dT$ was estimated from the temperature dependence of the yield stress in the temperature range from at 200 °C to be 0.159 MPa/K. The activation enthalpy calculated for 200 °C gives (0.95 ± 0.05) eV. Similar value of 0.96 eV has been reported for AX41 alloy (Trojanová et al. 2007). A rapid decrease of the flow stress at elevated temperatures indicates the possible occurrence of recovery process(-es) that is usually thermally activated. The values of the activation volume and the activation enthalpy may help to identify this thermally activated process. The activation of the prismatic slip and subsequent annihilation of the dislocation segments with the opposite sign have been found as the main reason for the observed internal stress decrease. The double cross slip and the thermally activated glide of the <c+a> dislocations in pyramidal planes should be taken into account. Because the values of the activation volume and activation energy are very

similar to that estimated for monolithic AX41 alloy, we can conclude that the thermally activated processes are the same.

4. Fracture properties

The observation of fracture surfaces may help to identify operating fracture mechanism (-s) of constituents at different temperatures and the bonding abilities of their interfaces. The fracture properties were studied on three materials: AZ91f (20vol.% Saffil), AZ91h (5% Saffil, 15% SiC, 3%Si) and AZ91p (10%SiC, 3% Si). The investigation was concentrated on the U-notch side of the fracture surface, where bending stresses are assumed to be generated during the impact testing. Specimens were fractured predominantly in a brittle manner even at 300 °C. The measured fracture energies were almost identical for all temperatures tested (about 1-2 J). This implies that on one hand the composite fibres/particles interfaces contribute to the stiffness, and on the other hand they serve as the crack initiators.

4.1 Fracture surfaces

AZ91f samples were slowly loaded in the three points bending with the aim to see the stable crack opening. The fracture mechanism is well seen in the scanning electron micrographs shown in Fig. 18a,b. The fibres plane is oriented perpendicular to the fracture surface. Fibres were pulled out on the fracture surface while in the side plane secondary cracks are visible. They cut the fibres lying perpendicular to the fracture surface and go around the other. The matrix (γ phase) is plastically deformed. The dimple morphology of the matrix is shown in Fig. 19a together with the bended fibres pulled out from the matrix. The similar dimple morphology of the fracture surface remained also after bending at 100 °C as it is demonstrated in Fig. 19b.

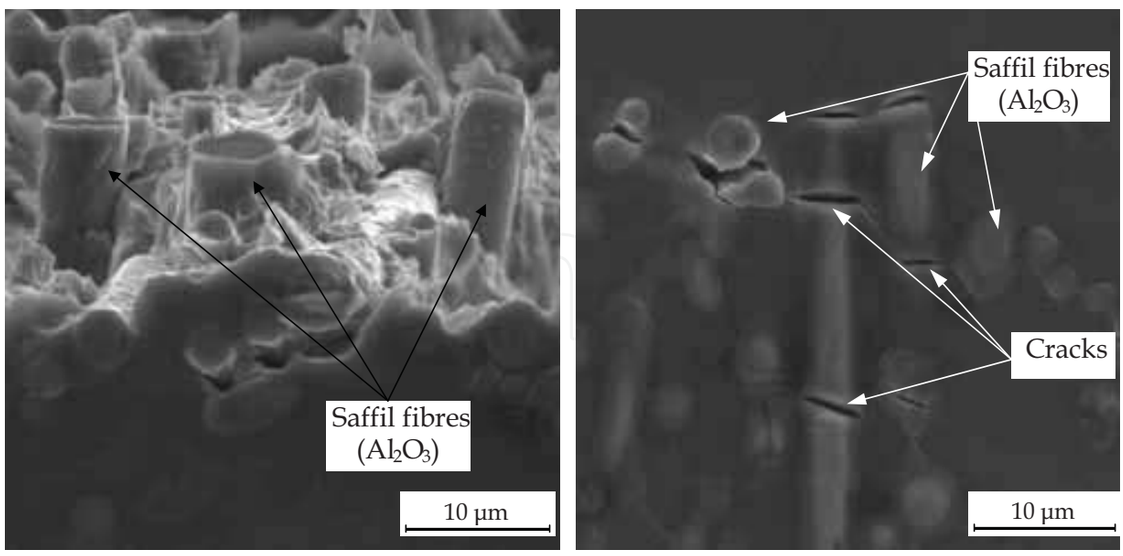

(a) (b)

Fig. 18. Detail of the fracture surface of AZ91f sample (a) and the secondary cracks at the side plane (b).

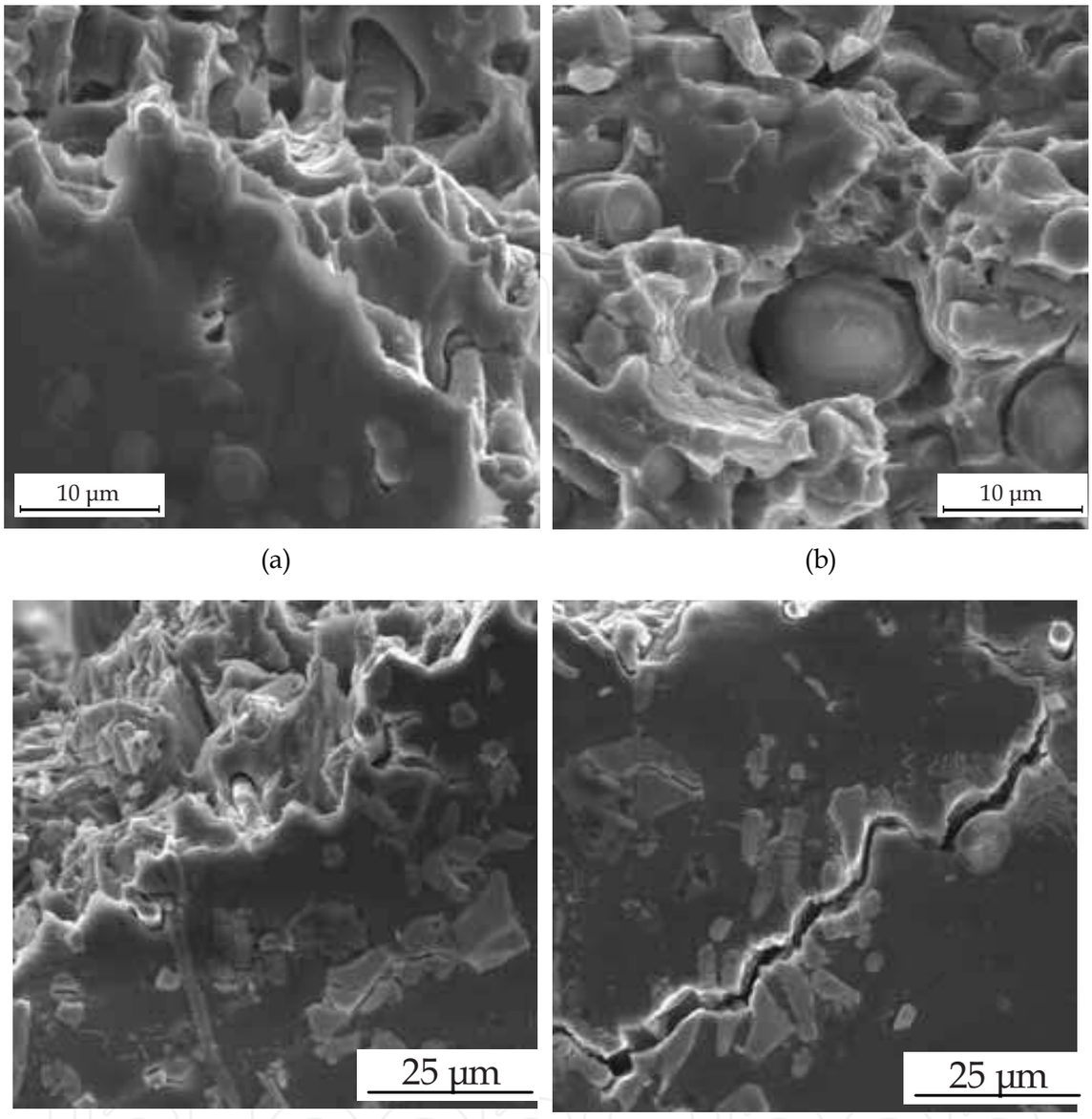

Fig. 19. Dimple morphology of the fracture surface of AZ91f sample (a) and fine dimples observed after bending at 100 °C (b). The crack formation in AZ91h sample (c). Reinforcing particles and fibres are the preferential places for the crack formation (d).

The formation of the fracture profile in the slowly bended AZ91h sample at ambient temperature is shown in Fig. 19c. Secondary cracks are created remote of the fracture surface in the vicinity of SiC particles and partially also Saffil fibres. The preferential places for the cracks formation are clusters of the reinforcing phase particles/fibres. Wang et al. studying the fracture properties of AZ91/SiC particles prepared by stir casting found that interface and particle segregation within the intergranular regions have their significant effect on thefracture behaviour of AZ91/ SiCp composite (Wang et al., 2007).

The matrix is deformed only slightly as it is demonstrated in Fig. 19d. Character of fracture surfaces and breakage of phases were almost identical for both composites AZ91f and AZ91h in the whole temperature range from 25 to 300 °C. During crack propagation, reinforcements serve as inhibitor of plastic deformation in the matrix. Moreover, the reinforcements are a source for formation of dimples and give originate to cracks. Separation at the matrix/reinforcement interface indicates weak bonding in the investigated temperature range (25-300 °C).
In addition, cleavage fracture of reinforcements was observed at lower temperatures (at RT and 100 °C). An increase of temperature causes also increase of plastic strain, which is responsible for debonding of reinforcements. The main features of the fracture surfaces of AZ91p samples in the investigated temperature range were similar: brittle fracture of SiCp and Mg_2Si phases (see Figs. 20) and slightly ductile fracture of the δ phase. Cracks were mostly initiated at the Mg_2Si phase (Fig.20).

4.2 Fracture mechanisms

Fracture of the γ phase in the AZ91f composite is transcrystalline ductile with dimples morphology with plastically transformed walls. The shape of walls depends on the orientation of Saffil fibres on fracture surface. At and above 200 °C slip bands were observed on the walls - depicted in Fig. 21 with the arrow, which correspond with the activity of non-basal dislocation glide. The γ phase is fractured by the transcrystalline cleavage mechanism (Fig. 22). Fine secondary microcracks were observed at temperatures between RT and 300 °C. Secondary microcracks are a result of the multiaxial plastic deformation in the matrix. Additionally, at and above 200 °C, complement fracture mechanism of γ phase arises simultaneously with transcrystalline cleavage mechanism; debonding at the interface γ phase/δ phase as well as γ phase/discontinuous precipitates occur and indicate interphase cleavage fracture. On the contrary, discontinuous precipitates were failed by the transcrystalline ductile fracture with the fine dimples morphology in the whole investigated temperature range.
In the AZ91p samples, coarse dendritic crystals and Chinese script particles failed by the transcrystalline cleavage fracture at all temperatures tested. The interface between the γ phase and the Mg_2Si is unlikely to be coherent since the lattice constants and the crystal structures are different. In spite of this, the bonding strength of the matrix/Mg_2Si interface is high as documented in Fig. 20a by comparison of the opposite surfaces of the fractured specimen. It appears that the development of crack within Mg_2Si coarse dendrites is easier than the debonding at the interface. The strong bonding between matrix and Mg_2Si may be a result of an "in situ" formation. Plastic deformation of the matrix and/or high velocity of main crack propagation may result in a large number of secondary cracks in the Mg_2Si coarse dendritic crystals as observed in Fig. 20. The second main contribution to the crack propagation comes from SiC particles. Fracture mechanisms did not change throughout the temperature range RT to 300 °C. In comparison with Mg_2Si, SiC particles cracks are developed mainly by the delamination of interfaces with the Mg matrix. However, trancrystalline cleavage fracture was observed as well.
Minor contributions to the crack propagation are from the γ phase, the γ phase and the discontinuous precipitates (Fig. 23). The transcrystalline cleavage of the γ phase with secondary microcracks and the transcrystalline ductile fracture with the fine dimples morphology of the discontinuous precipitates (γ+δ) were observed in the entire investigated

temperature range. The nature of γ phase fracture varied with temperature (Fig.23a,b) but this change was not significant; generally the higher the temperature the more plastic fracture surface, which corresponds with anticipated activity of other slip systems at higher temperatures (~ 200 °C).

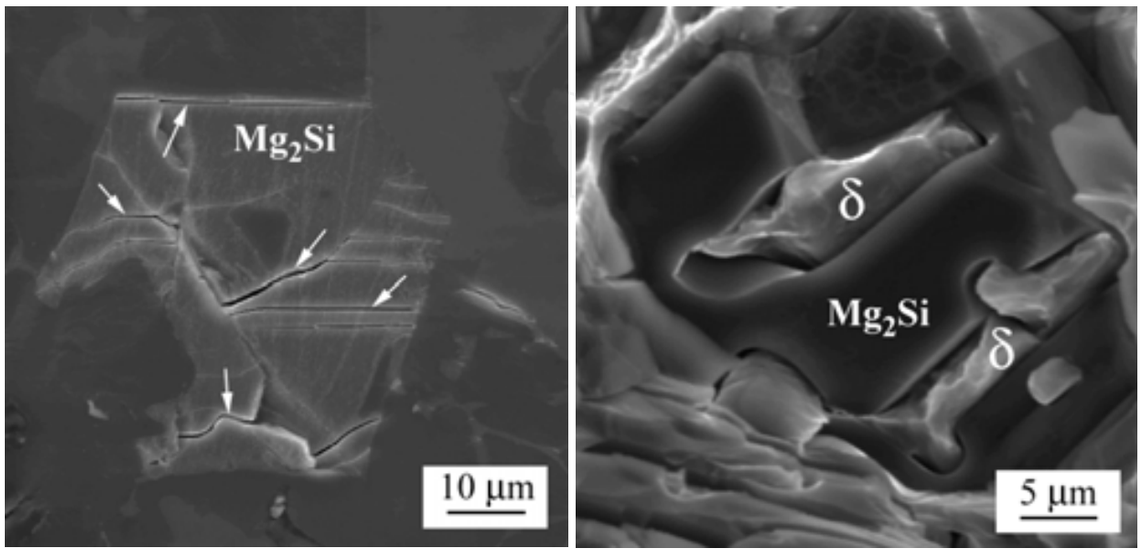

(a) (b)

Fig. 20. Microcracks (arrows) between matrix and SiC particles near the fracture surface in AZ91p sample after impact test at RT (a), brittle fracture of SiCp after test at 300 °C (b).

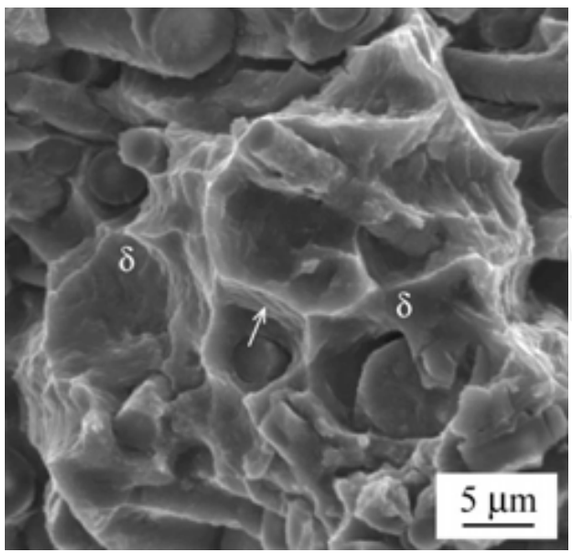

Fig. 21. Fracture surface of AZ91f after impact test at 300 °C.

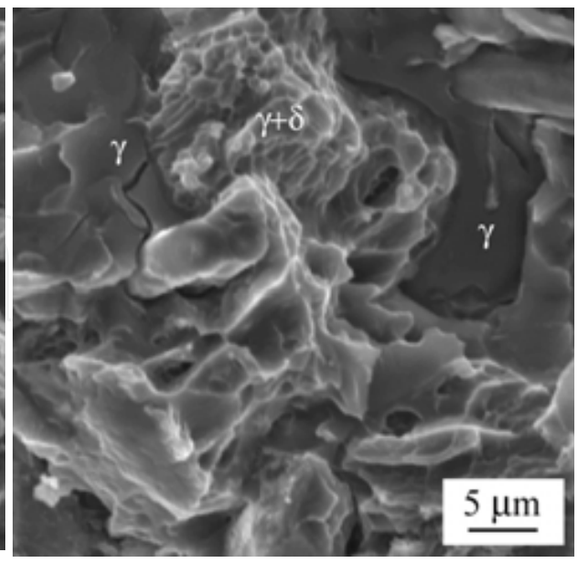

Fig. 22. Fracture surface of AZ91h sample after impact test at 200 °C.

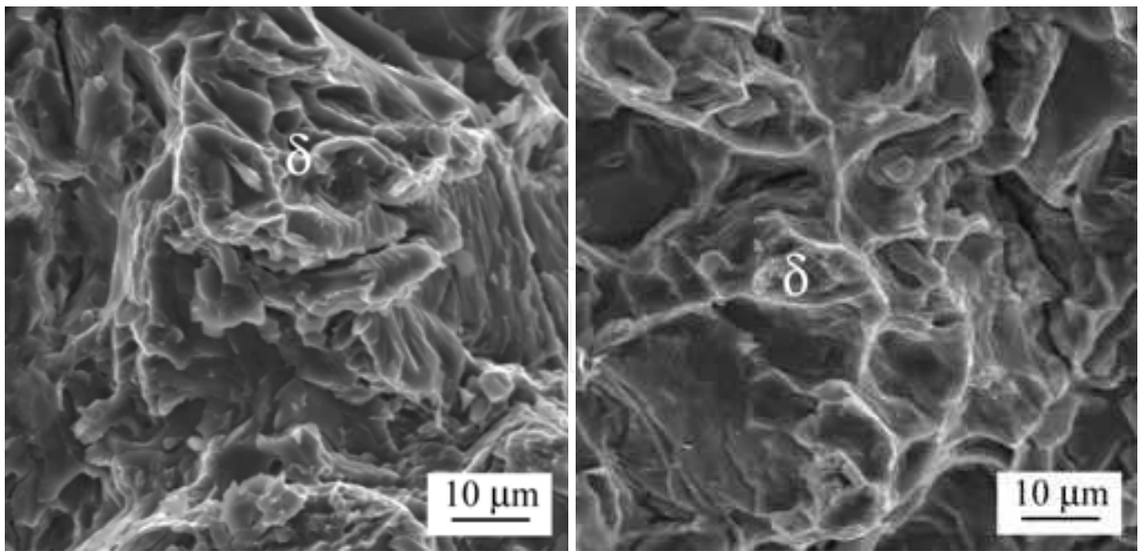

(a) (b)

Fig. 23. Comparison of γ phase breakage at RT (a) and 300 °C (b), mechanism for both is transcrystalline ductile fracture with plastically transformed walls.

The fracture mechanism was identified as transcrystalline ductile with dimples morphology accompanied by plastically transformed walls. As temperature increased the walls become higher and the dimples spread out. However, in comparison with AZ91f and AZ91h samples the plasticity of walls with temperature change is not as significant as in the case of AZ92f and AZ91h composites. Furthermore, slip bands were not observed on the walls at higher temperatures. The most probable reason for such behaviour is that brittle components present in considerable amount impede the plastic straining of the relatively ductile matrix. The increased plasticity of the matrix with temperature rise is in agreement with the deformation behaviour.

Concluding remarks

The Mg alloys based composites studied is very brittle at all temperatures as proved by impact tests. The fracture mechanism of Mg-MMCs was controlled by fiber/matrix interface and fiber breakage (see also Hu et al., 2010). The Mg matrix exhibits a slightly plastically deformed fracture surface at and above 200 °C.

5. Acknowledgements

The authors dedicate this paper to Prof. RNDr. František Chmelík, CSc, on the occasion of his 50th birthday. This work received a support from the Ministry of Education, Youth and Sports of the Czech Republic by the project MSM 0021620834.

6. References

Aikin, Jr. R.M. & Christodoulou, L. (1991). The role of equiaxed particles on the yield stress of composites. *Scripta Metall. Mater.*, 25, 1991, 9-14. ISSN: 1359-6462.

Arsenault, R.J. & Fisher, R. (1983). Microstructure of fiber and particulate SiC in 6061 Al composites. *Scripta Metall.*, *17*, 67-71, ISSN: 1359-6462

Arsenault, R.J. & Shi, N. (1986). Dislocation generation due to differences between the coefficients of thermal expansion. *Mater. Sci. Eng.*, *81*, 175-187. ISSN: 0254-0584.

Ashby, M.F. (1993). Criteria for selecting the components of composites. *Acta Metall. Mater.*, *41*, 1313-325. ISSN: 1359-6454.

Carreño-Morelli, E.; Urreta, S.E. & Schaller, R. (2000). Mechanical spectroscopy of thermal stress relaxation at metal–ceramic interfaces in aluminium-based composites. *Acta Mater.*, *48*, 4725-4733. ISSN: 1359-6454.

Clyne, T.W. & Withers, P.J. (1993). *An Introduction to Metal Matrix Composites*, Cambridge Univ. Press, Cambridge. ISBN 0-521-41808-9.

Delannay, F. (2000). *Thermal stresses and thermal expansion in MMCs.* pp. 341-369. In: Clyne T.W. Ed.. Comprehensive composite materials, Vol. 3. Amsterdam, Elsevier 341. ISBN:903761-04-2.

Dieringa, H.; Hort, H. & Kainer, K.U. (2005) The "AZo Journal of Materials Online"*AZojomo* 1 1–10; DOI:10.2240/azojomo0117.
http://www.azom.com/details.asp?ArticleID=2984,

Feltham, P. (1963) Stress relaxation in magnesium at low temperatures. *Phys. Stat. Sol.* 3. 1340–1346. ISSN: 1862-6300.

Kapoor, R.; Wadekar, S.L. & Chakravartty, J.K. (2002). Deformation in Zr-1Nb-1Sn-0.1 Fe using stress relaxation technice. *Mater. Sci. Eng. A,* 328, 324–333. ISSN: 0921-5093.

Kocks, U.F.; Argon, A.S. & Ashby, M.F. (1975). Thermodynamics and kinetics of slip. *Progr. Mater. Sci*., 19, 1–288. ISSN: 0079-6425.

Lilholt, H. (1991). Aspects of deformation of metal matrix composites. *Mater. Sci. Eng. A*, 161-171. ISSN: 0921-5093.

Lloyd, D.J. (1994). Particle-reinforced aluminum and magnesium matrix composites. *Int. Mater. Rev. 39* 1-23. ISSN: 0950-6608.

Li, J.M.C. (1967) Dislocation dynamics in deformation and recovery *Canad. J. Appl. Phys.* 45 493–509. ISSN : 0008-4204..

Miller, W.S. & Humphreys, F.J. (1991). Strengthening mechanism in particulate metal matrix composites. *Scripta Metall. Mater.,* 25, 33-38. ISSN: 1359-6462.

Ono, K. (1968). Temperature dependence of dispersed barrier hardening. *J. Appl. Phys.* 39, 1803–1806. ISSN: 0021-8979.

Z. Száraz, Z. Trojanová, M Cabbibo, M. & Evangelista, E. (2007). Strengthening in a WE54 magnesium alloy containing SiC particles. *Mater. Sci. Eng. A, 462*, 225-229. ISSN: 0921-5093.

Lukáč, P. & Balík, J. (1994). Kinetics of plastic deformation. *Key Engn. Mater*., 97-98, 307-322. ISBN: 0-87849-687-4.

Trojanová, Z.; Drozd, Z.; Kúdela, S.; Száraz, Z. & Lukáč, P. (2007). Strengthening in Mg-Li matrix composites. *Comp. Sci. Tech.,* 67, 1965-1973. ISSN: 0266-3538 .

Trojanová, Z.; Gärtnerová, V.; Drozd, Z.; Száraz, Z. & Lukáč, P. (2008). Short fibres and particles impact on compressive behaviour of an AZ91 alloy. *Int. Foundry Res*., 60, 44-52. ISSN: 0046-5933.

Trojanová, Z.; Gärtnerová, V.; Lukáč, P. & Drozd, Z. (2004). Mechanical properties of Mg alloys composites reinforced with short Saffil fibres. *J. Alloys Comp.* 378, 19-26. ISSN: 0266-3538.

Trojanová, Z., Lukáč, P. & Kainer, K.U. (2007) Stress relaxation in AX41 magnesium alloy studied at elevated temperatures. *Advanced Engn. Mater*. 9, 370-374. ISSN: 1438-1656.

Wang, X.J.; Wu, K.; Huang, W.X.; Zhang, H.F.; Zheng, M.Y. & Peng D.L. (2007).. Study on fracture behavior of particulate reinforced magnesium matrix composite using in situ SEM. *Comp. Sci. Tech.* 67 2253–2260. ISSN: 0266-3538.

Hu, B.; Peng, L.; Powell, B.R.; Balough, M.P.; Kubic, R.C. & Sachdev, A.K. (2010). Interfacial and fracture behavior of short-fibers reinforced AE44 based magnesium matrix composites. *J. Alloys Comp.* 504, 527-534. ISSN: 0925-8388.

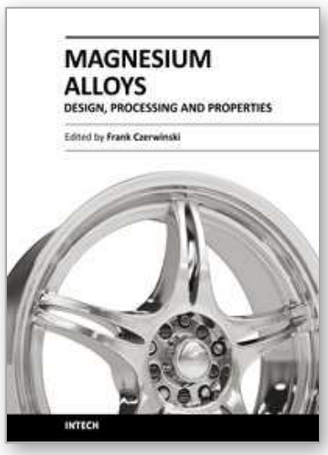

Magnesium Alloys - Design, Processing and Properties

Edited by Frank Czerwinski

ISBN 978-953-307-520-4
Hard cover, 526 pages
Publisher InTech
Published online 14, January, 2011
Published in print edition January, 2011

Scientists and engineers for decades searched to utilize magnesium, known of its low density, for light-weighting in many industrial sectors. This book provides a broad review of recent global developments in theory and practice of modern magnesium alloys. It covers fundamental aspects of alloy strengthening, recrystallization, details of microstructure and a unique role of grain refinement. The theory is linked with elements of alloy design and specific properties, including fatigue and creep resistance. Also technologies of alloy formation and processing, such as sheet rolling, semi-solid forming, welding and joining are considered. An opportunity of creation the metal matrix composite based on magnesium matrix is described along with carbon nanotubes as an effective reinforcement. A mixture of science and technology makes this book very useful for professionals from academia and industry.

InTech Europe
University Campus STeP Ri
Slavka Krautzeka 83/A
51000 Rijeka, Croatia
Phone: +385 (51) 770 447
Fax: +385 (51) 686 166
www.intechopen.com

InTech China
Unit 405, Office Block, Hotel Equatorial Shanghai
No.65, Yan An Road (West), Shanghai, 200040, China
中国上海市延安西路65号上海国际贵都大饭店办公楼405单元
Phone: +86-21-62489820
Fax: +86-21-62489821

IntechOpen